record (since 1980). Ida's destruction was unique in that its damage was concentrated in two distinct regions. It made landfall as a powerful Category 4 storm in Louisiana, causing heavy damage to the Gulf Coast. As Ida's remnants moved northward, it merged with a frontal system to produce severe weather and flash flooding in the mid-Atlantic states and Northeast, with especially significant impacts in areas of Pennsylvania, New Jersey, and New York. Sidebar 4.1 provides more details on Ida's meteorological history and records.

Table 4.2. Global counts of TC activity by basin for 2021. "+" denotes top tercile; "++" is top 10%; "–" is bottom tercile; "––" is bottom 10% (all relative to 1991–2020). (Note that some inconsistencies between Table 4.2 and the text of the various basin write-ups in section 4g exist and are unavoidable, as tallying global TC numbers is challenging and involves more than simply adding up basin totals, because some storms cross TC basin boundaries, some TC basins overlap, and multiple agencies are involved in tracking and categorizing TCs.)

Basin	TCs	HTCs	Major HTCs	SS Cat 5	ACE ($\times 10^4$ kt^2)
North Atlantic	21 ++	7	4 +	0	146
Eastern Pacific	19 +	8	2 –	0	94 –
Western Pacific	23 –	10 ––	5 –	4 +	209 –
North Indian	5	3 +	1 +	0	21
South Indian	12 +	5	2 –	1 ++	100
Australia	12 +	3 –	2	1 ++	44 –
Southwest Pacific	9 +	4	2	1 ++	41
Global Totals	**97** **+**	**38** **––**	**17** **––**	**7** **+**	**656** **–**

2) ATLANTIC BASIN—M. Rosencrans, E. S. Blake, C. W. Landsea, H. Wang, S. B. Goldenberg, and R. J. Pasch

(i) 2021 Seasonal activity

The 2021 Atlantic hurricane season produced 21 named storms, of which 7 became hurricanes and 4 of those became major hurricanes (Fig. 4.22b). The HURDAT2 (Landsea and Franklin 2013) 1991–2020 seasonal averages (included in IBTrACS) are 14.4 named storms, 7.2 hurricanes, and 3.2 major hurricanes. The 21 named storms during 2021 were the third most on record, trailing the 30 named storms in 2020 and 28 in 2005. Eight of the 21 named storms during 2021 were short-lived (≤ 2 days). There has been a large increase (approximately five per year) in detection of these "shorties" since 2000 (Landsea et al. 2010; Klotzbach et al. 2022). These increased counts primarily reflect new observational capabilities such as scatterometers, Advanced Microwave Sounding Units, and the Advanced Dvorak Technique, and have no association with any known climate variability (Villarini et al. 2011).

The 2021 seasonal Accumulated Cyclone Energy (ACE) value was 149.2% of the 1951–2020 median (which is 96.7×10^4 kt^2; Fig. 4.22c). This value was the 13th highest since 1970 and above NOAA's threshold for an above-normal season (126.1×10^4 kt^2, or 130% of median). There have now been a record six consecutive above-normal seasons, extending the current record of five. Since the current Atlantic high-activity era began in 1995 (Goldenberg et al. 2001; Bell et al. 2019, 2020), there have been 17 above-normal seasons, with 10 of those considered extremely active (ACE ≥ 165% of median, also referred to as hyperactive). By comparison, the preceding 24-year low-activity era of 1971–94 had only two above-normal seasons with none extremely active.

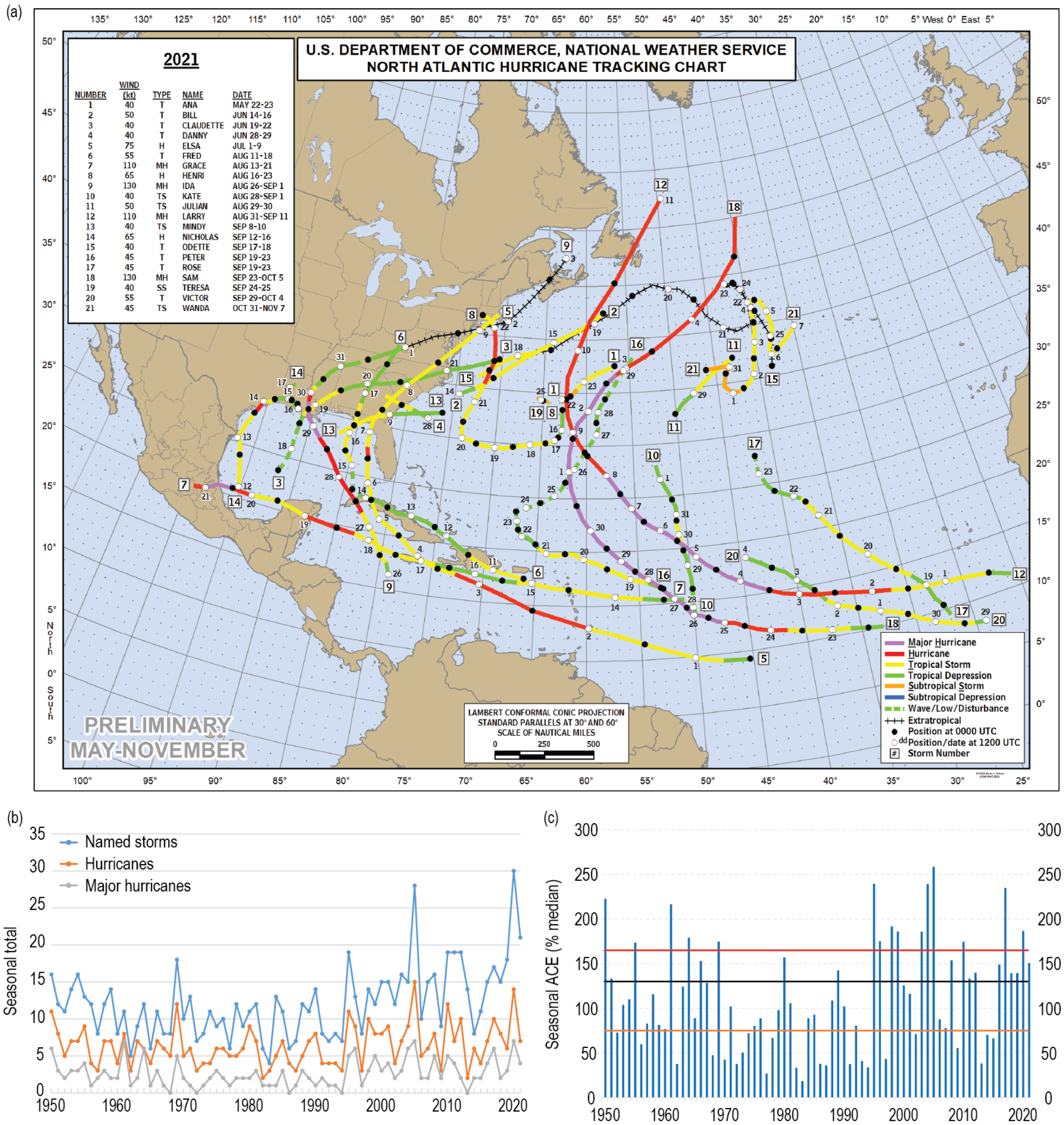

Fig. 4.22. (a) 2021 Atlantic basin storm tracks. Seasonal Atlantic hurricane activity during 1950–2021 for (b) numbers of named storms (blue), hurricanes (orange), and major hurricanes (gray) and (c) the Accumulated Cyclone Energy (ACE) index expressed as percent of the 1951–2020 median value. ACE is calculated by summing the squares of the 6-hourly maximum sustained surface wind speed (kt) for all periods while the storm is at least tropical storm strength. The black (orange) line represents NOAA's limit for an above-normal (below-normal) season and the red line is the threshold for an extremely- (aka hyper-) active season, (http://www.cpc.ncep.noaa.gov/products/outlooks/ background_information.shtml). Note that there is a low bias in activity from the 1950s to the early 1970s due to the lack of satellite imagery and technique (Dvorak) to interpret tropical cyclone intensity for systems over the open ocean. (Source: HURDAT2 [Landsea and Franklin 2013].)

(ii) Storm formation times, regions, and landfalls

Tropical cyclone (TC) activity occurred throughout most of the 2021 hurricane season (Fig. 4.23b), with a TC present every month in the official season as well as in May. Activity ramped up relatively quickly, with Elsa becoming the earliest developing fifth named Atlantic storm on record when it formed on 1 July. Of the first five named storms in the 2021 Atlantic hurricane season, four were classified as a "shortie", lasting two days or fewer. On average, 1–2 named storms form per year during May–July.

August–October (ASO), typically the most active part of the hurricane season, featured 16 named storms during 2021 compared with the 1991–2020 average of 11.1, and at least one TC was present at all times from mid-August through early October. Six of these 16 storms became hurricanes (the seventh hurricane of the season, Elsa, formed in July), and four of those became major hurricanes. Most of these ASO storms (9 of 16) formed in the main development region (MDR), which is also typical of an above-normal season. The MDR spans the tropical Atlantic Ocean and Caribbean Sea between 9.5°N and 21.5°N (Goldenberg and Shapiro 1996; Goldenberg et al. 2001; Bell and Chelliah 2006; Bell et al. 2017, 2018, 2019). After a highly active late August and most of September, Atlantic TC activity dropped precipitously, with only one named storm developing after 29 September. Tropical Storm Wanda was first named as a subtropical storm on 31 October, gaining tropical characteristics in early November, ending a nearly month-long quiet period.

Historically, above-normal seasons result from a sharp increase in the number, intensity, and duration of storms that develop in the MDR. For the entire 2021 season, 10 of the 21 named storms formed in the MDR (Fig. 4.23a) and accounted for five of the season's seven hurricanes and all of the season's four major hurricanes. The associated MDR-related ACE value was 129% of the basin-wide median. By comparison, named storms forming in the Gulf of Mexico only contributed 5% of the basin-wide median in 2021, and storms from the extratropics contributed 15%. This MDR-related ACE value is lower than the 1991–2020 MDR average for above-normal seasons of 140% of the median. These values are roughly five times higher than the MDR average of 20% of the median for below-normal seasons (defined by NOAA as having a total basin-wide ACE less than 73×10^4 kt^2).

The actual storm tracks during 2021 (Fig. 4.22a) showed two main regions of activity. One area was oriented from west-southwest to east-northeast across the extratropics, where eight named storms formed. The MDR was also active, but in the middle of these active areas there was a quiet area in the extreme southwest Atlantic including the east coast of Florida and the Bahamas.

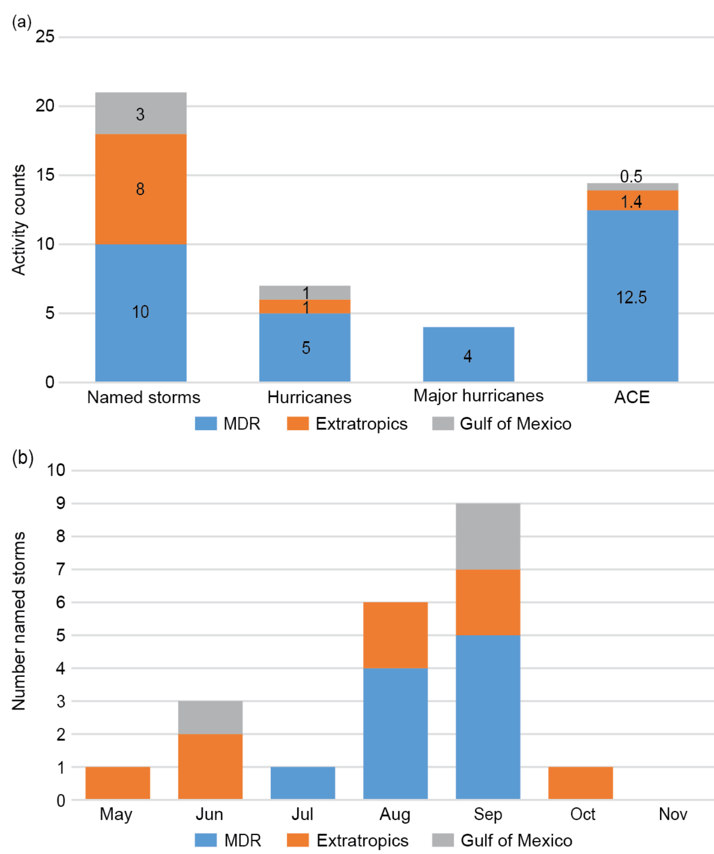

Fig. 4.23. Atlantic TC activity in 2021. (a) Total seasonal storm counts for the three storm classifications and for ACE shown for each region the storm was first named. (b) Named storm counts shown for the month and region the storm was first named. ACE reflects the entire storm ACE and is attributed to the region in which the storm was first named. Regions in (a) and (b) are indicated by the color bar below panel (b). The Atlantic MDR spans 20°–87.5°W and 9.5°–21.5°N. The "extratropics" includes all regions except for the MDR and Gulf of Mexico. (Source: HURDAT2 [Landsea and Franklin 2013].)

Several of the MDR formations have long tracks to the west-northwest. The season also featured eight storms making landfall in the continental United States, with others impacting the Caribbean, Mexico, Central America, Newfoundland, and Bermuda.

Several notable individual storms formed during the 2021 hurricane season. Hurricane Sam was a major hurricane for 7.75 days, contributing ~38% of the total seasonal ACE. Fortunately, Sam's track remained out to sea with minimal impacts. In terms of damage, Hurricane Ida was the largest disaster for the United States in 2021, causing $75 billion (U.S. dollars). Preliminary estimates indicate Ida had winds of 130 kt as it made landfall in Louisiana, which would be tied for the fifth-strongest hurricane to make landfall in the United States since more reliable records began around 1900. In addition to significant damage along the Gulf Coast, Ida also interacted with a cold front to produce torrential rain and flooding across the mid-Atlantic and Northeast. More information on Hurricane Ida is detailed in Sidebar 4.1. Hurricane Henri also brought significant rains to the Northeast just a week earlier, establishing some localized daily records but no large regional records, and causing an estimated $700 million (U.S. dollars) in damage. Hurricane Grace spread damage across the Caribbean and into Mexico, causing an estimated $300 million (U.S. dollars) in damage. Tropical Storms Elsa and Fred and Hurricane Nicholas were storms that each caused more than $1 billion (U.S. dollars) in damage (see section 7b2).

(iii) Sea surface temperatures

Four main sea surface temperature (SST) signals were present during ASO 2021 (Fig. 4.24). First, SSTs were above average throughout the MDR (Fig. 4.24a), and the area-averaged SST anomaly was +0.35°C (Fig. 4.24b). The largest anomalies in the MDR were observed throughout the Caribbean Sea and ranged from just above 0°C to +0.5°C.

Second, the area-averaged SST anomaly in the MDR was higher (by +0.17°C) than that of the remainder of the global tropics (Fig. 4.24c). This signal typifies the warm phase of the Atlantic multi-decadal oscillation (AMO; Enfield and Mestas-Nuñez 1999; Bell and Chelliah 2006) and is a ubiquitous characteristic of Atlantic high-activity eras, such as 1950–70 and 1995–present (Goldenberg et al. 2001; Vecchi and Soden 2007; Bell et al. 2018).

The third SST signal during ASO 2021 reflected above-average temperatures across most of the North Atlantic Ocean. Outside of the MDR, the largest anomalies (exceeding +1°C) occupied the western, and portions of the central, North Atlantic (Fig. 4.24a), areas where numerous tropical storms and hurricanes tracked. The area-averaged SST anomaly in the western North Atlantic (red box, Fig. 4.24a) was +0.79°C and reflected a continuation of exceptional warmth that began in 2014 (Fig. 4.24d).

The fourth SST signal during ASO 2021 was the development of La Niña in the equatorial Pacific (section 4b). As discussed below, La Niña contributed to the enhanced hurricane activity during August and September.

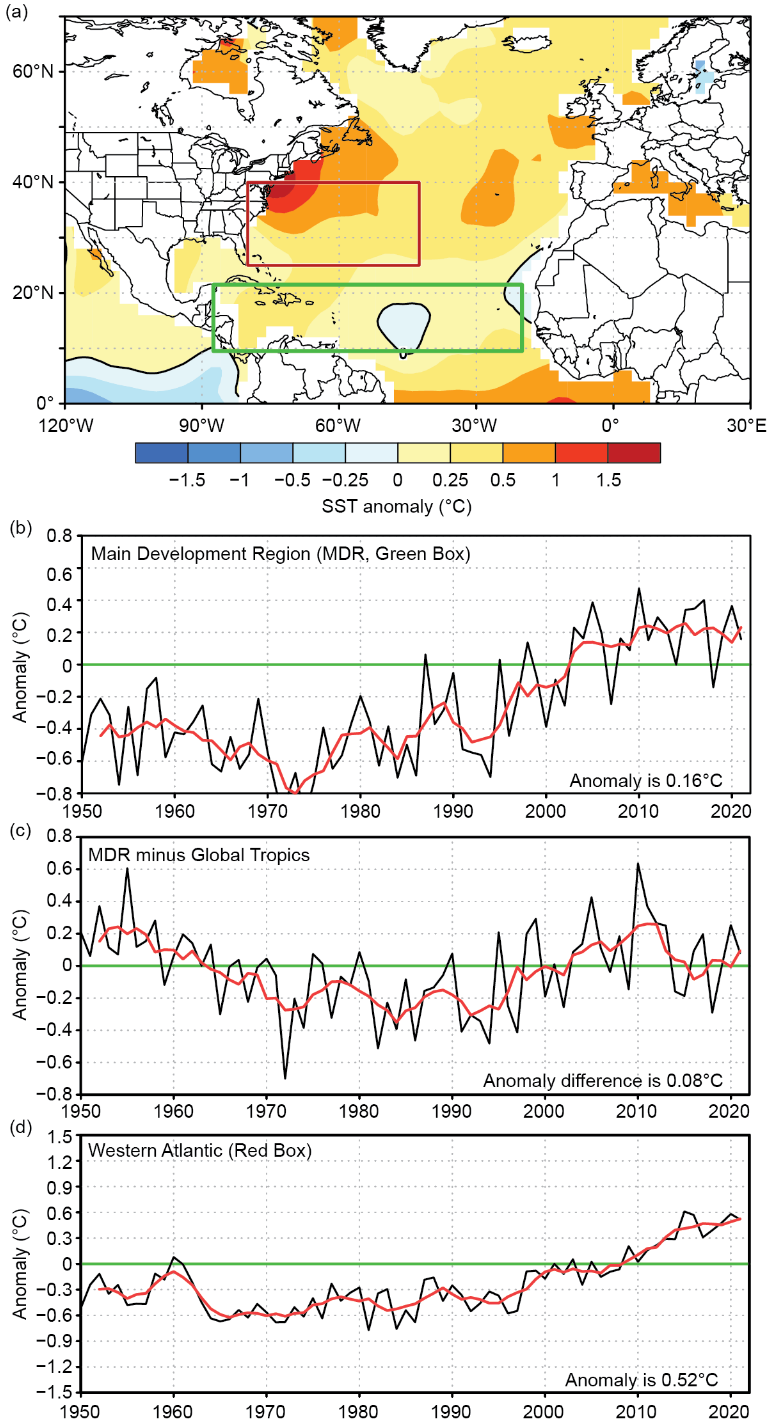

Fig. 4.24. (a) Aug–Oct 2021 SST anomalies (°C). (b–d) Time series of Aug–Oct area-averaged SST anomalies (black) and 5-pt running mean of the time series (red); (b) In the MDR (green box in (a) spanning 20°–87.5°W and 9.5°–21.5°N); (c) difference between the MDR and the global tropics (20°S–20°N); and (d) in the western North Atlantic (red box in (a) spanning 42.5°–80°W and 25°–40°N). Anomalies are departures from the 1991–2020 period means. (Source: ERSST-v5 [Huang et al. 2017].)

(iv) Atmospheric conditions

Climatologically, the ASO peak in Atlantic hurricane activity largely reflects the July–September (JAS) peak in the West African monsoon as noted in section 4e. The inter-related circulation features of an enhanced monsoon act to further increase hurricane activity, while those with an anomalously weak monsoon act to suppress it (Gray 1990; Hastenrath 1990; Landsea et al. 1992; Bell and Chelliah 2006; Bell et al. 2018, 2020). The association on multi-decadal time scales between the West African monsoon and Atlantic hurricane activity largely exists because of a common relationship to multi-decadal modes of variability (Bell and Chelliah 2006).

The West African monsoon was enhanced during JAS 2021, as indicated by negative outgoing longwave radiation (OLR) anomalies across the African Sahel (red box, Fig. 4.25a). Total OLR values in this region averaged 239 W m^{-2} (Fig. 4.25b), with values less than 240 W m^{-2}, indicating deep tropical convection. Consistent with these conditions, the larger-scale divergent circulation at 200-hPa featured an extensive area of anomalous divergence and a core of negative velocity

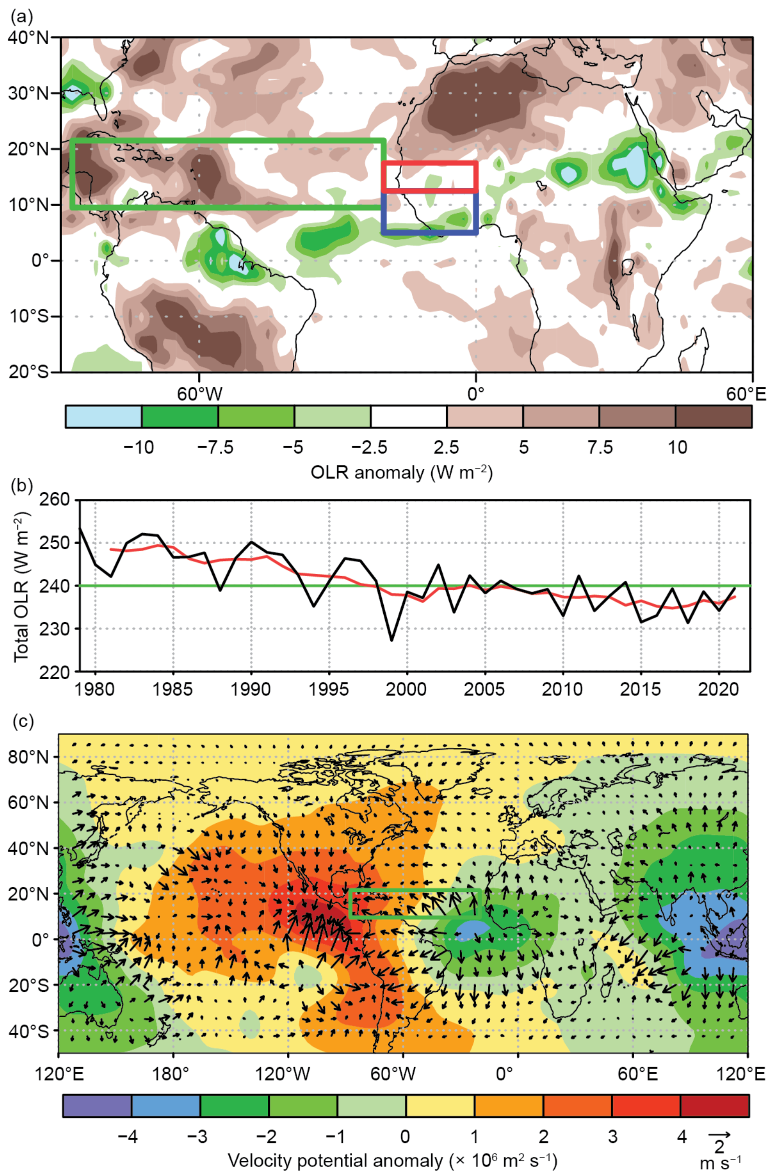

Fig. 4.25. (a) Jul–Sep 2021 anomalous OLR (W m^{-2}), with negative (positive) values indicating enhanced (suppressed) convection. (b) Time series of Jul–Sep total OLR (black) and 5-pt running mean of the time series (red) averaged over the African Sahel region (red box in (a, c) spanning 20°W–0° and 12.5°–17.5°N). (c) Aug–Oct 2021 anomalous 200-hPa velocity potential (× 10^6 m^2 s^{-1}) and divergent wind vectors (m s^{-1}). In (a), contours show total OLR values of 220 W m^{-2} and 240 W m^{-2}. In (a, c), the green box denotes the Atlantic MDR. Anomalies are departures from the 1991–2020 means. (Sources: NCEP/NCAR Reanalysis [Kalnay et al. 1996] for velocity potential and wind, and Liebmann and Smith [1996] for OLR.)

potential anomalies across subtropical northern Africa extending into the eastern Atlantic (Fig. 4.25c). The OLR time series shows that an enhanced monsoon has largely prevailed throughout the current Atlantic high-activity era and warm AMO of 1995–present (Fig. 4.25b). By contrast, a much weaker monsoon with OLR values well above 240 W m^{-2} in the Sahel region was typical of the low-activity and cool AMO period from 1971 to 1994. During ASO 2021, core atmospheric conditions within the MDR reflected a combination of the enhanced West African monsoon, La Niña, and midlatitude influences.

At 200-hPa, the enhanced monsoon amplified subtropical ridges (indicated by anticyclonic streamfunction anomalies) across Africa in both hemispheres (Fig. 4.26a). La Niña impacts in that field (Bell and Chelliah 2006) included cyclonic streamfunction anomalies in both hemispheres of the western and central subtropical Pacific. Farther north, a large anticyclonic anomaly was evident over eastern Canada. Troughing extended from northern Mexico, across Florida, and into the central extratropical Atlantic near 40°N. The streamfunction pattern over the western and central subtropical Pacific aligns with the La Niña response identified in Bell and Chelliah (2006), while the cyclonic streamfunction anomalies over northern Mexico, across Florida, and into the extratropical Pacific are dissimilar to that identified response pattern, pointing to some other source of variability having influence over those regions. The 1000-hPa anomalous height and wind field (Fig. 4.26c) showed just how strong some of the midlatitude circulations were and even shows evidence of flow deep into the tropics. Sea level pressure was also below normal over the central and eastern MDR, which would typically correspond to decreased wind shear and more convection, but vertical wind shear was near normal for the season, and OLR indicates slightly above-normal convection.

The West African monsoon was enhanced and showed direct influences on the circulation pattern during ASO 2021. An aspect of the enhanced West African monsoon system during ASO 2021 was an upward extension of the westerly wind anomalies over the eastern half of the MDR to at least 700-hPa (Fig. 4.26d), which is the approximate level of the African Easterly Jet (AEJ). This anomaly pattern contributed to a deep layer of anomalous cyclonic relative vorticity (i.e., increased horizontal cyclonic shear) along the equatorward flank of the AEJ. These conditions are known to favor increased TC activity by helping African easterly waves to be better maintained

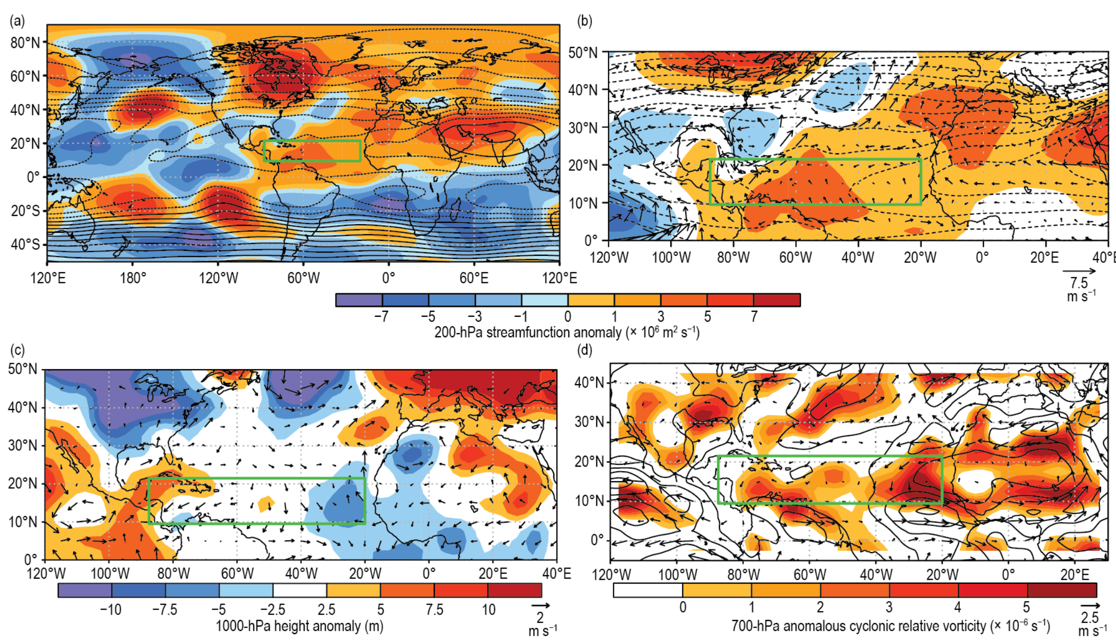

Fig. 4.26. Aug–Oct 2021: (a) 200-hPa streamfunction (contours, interval is 5 × 10^6 m^2 s^{-1}) and anomalies (shaded), with anomalous vector winds (m s^{-1}) also shown in (b); (c) anomalous 1000-hPa heights (shaded, m) and vector winds; and (d) anomalous 700-hPa cyclonic relative vorticity (shaded, × 10^6 m^2 s^{-1}) and vector winds. Green box denotes the MDR. Anomalies are departures from the 1991–2020 means. (Source: NCEP/NCAR Reanalysis [Kalnay et al. 1996].)

and by providing an inherent cyclonic rotation to their embedded convective cells (Bell et al. 2020; Landsea et al. 1998).

The anomalous low-level circulation also reflected an extensive flow of deep tropical moisture into the southern half of the central and eastern MDR. This moisture not only helps feed the monsoon, but also favors increased Atlantic hurricane activity. This situation contrasts with the drier and cooler air that normally accompanies enhanced northeasterly trade winds when the monsoon is weak.

The ASO 2021 200–850-hPa vertical wind shear was about average for much of the MDR and slightly higher than average for the western MDR/Caribbean (Fig. 4.27a). The area-averaged magnitude of the vertical wind shear for the entire MDR was 9.4 m s^{-1} (Fig. 4.27b) and for the Gulf of Mexico was 10.4 m s^{-1} (Fig. 4.27c). Both of these values are above the upper threshold of 8 m s^{-1} considered conducive to hurricane formation on monthly time scales (Bell et al. 2017), so the above-normal overall activity is even more remarkable. The sharp peak and busy month of September, in which nine named storms developed (Fig. 4.23b), was coincident with a period of anomalously low vertical wind shear in the MDR (Fig. 4.27d). The abrupt end to the season, with only one storm developing after 29 September, coincided with a period of anomalously strong wind shear across the Gulf of Mexico, Caribbean, MDR, and the extratropical Atlantic.

The MJO (Madden and Julian 1971), as discussed in section 4c, was generally stationary and inactive during September and October. Nonetheless, variations in the large-scale tropical convection may have played a role in the quiescent October. From September to October, the main convective activity shifted from the Indian Ocean to the Maritime Continent, as assessed via a combination of the multivariate MJO index of Wheeler and Hendon (2004; Fig. 4.8d) and Climate Prediction Center's weekly MJO analysis. For a typical MJO, this circulation results in increased shear over and decreased convection in the tropical Atlantic (Mo 2000), both of which decrease

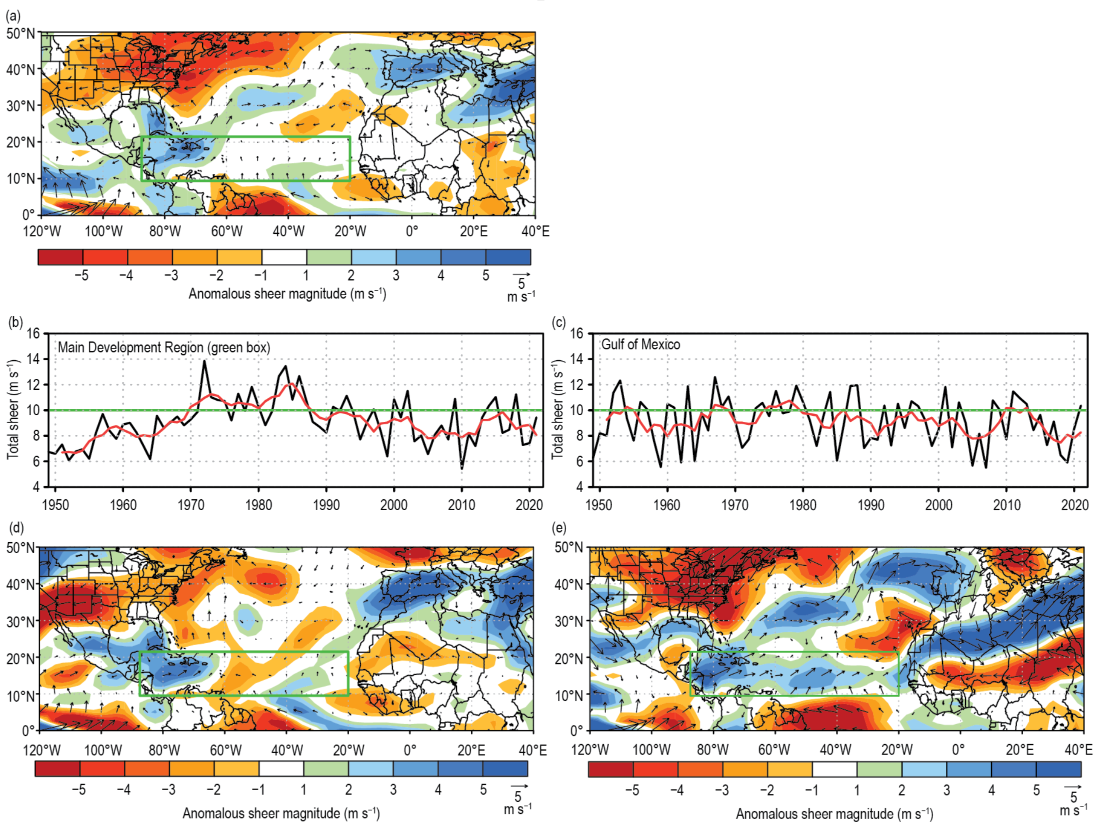

Fig. 4.27. Aug–Oct (ASO) magnitude of the 200–850-hPa vertical wind shear (m s^{-1}): (a) 2021 anomalous magnitude and vector. (b, c) Time series of ASO vertical wind shear magnitude (black) and 5-pt running mean of the time series (red) averaged over (b) the MDR (spanning 87.5°–20°W and 9.5°–21.5°N), and (c) the western Gulf of Mexico (spanning 80°–97.5°W and 21.5°–30°N). (d) Same as (a), but for Sep 2021. (e) Same as (d), but for Oct 2021. Anomalies are departures from the 1991–2020 means. (Source: NCEP/NCAR Reanalysis [Kalnay et al. 1996].)

tropical cyclone formations. Even if this were not a typical MJO, the shift in the variations of the tropical circulation may have contributed to the lack of activity in October.

The above conditions typified the many active seasons seen during the current Atlantic high-activity era. However, as with other years, interannual signals were also in play during 2021. One of those was La Niña, which favors enhanced activity as in other recent La Niña events (2010, 2016, and 2020). However, the La Niña impact may have been reduced by other interannual signals like the strong ridge over eastern Canada (Figs. 4.26a,c) with troughing over the central extratropical Atlantic and over the Gulf of Mexico. The ridge/trough combinations likely contributed to increased wind shear, especially late in the season, which may have capped activity, despite the presence of many features of the high-activity era (above-normal SST, enhanced West African Monsoon, and early season activity).

Sidebar 4.1: Hurricane Ida: A landfalling Louisiana major hurricane for the record books—P. KLOTZBACH AND R. TRUCHELUT

The 2021 Atlantic hurricane season was the sixth consecutive above-average season based on NOAA's definition, with 21 named storms, seven hurricanes, and four major hurricanes. Eight named storms and two hurricanes made landfall in the continental United States, with Hurricane Ida by far the most significant landfalling Atlantic tropical cyclone of the year. Ida struck near Port Fourchon, Louisiana, with maximum 1-minute sustained winds of 130 kt (67 m s^{-1}) on 29 August. Wind and surge caused tremendous destruction in south-central and southeastern Louisiana, with the New Orleans metropolitan area also experiencing significant wind damage. Ida's remnants interacted with a frontal system to cause significant flash flooding across the coastal plain of the northeastern United States, including Pennsylvania, New Jersey, New York, and Connecticut. The National Hurricane Center's best track report on Hurricane Ida (Beven et al. 2022) estimated that Ida caused ~$75 billion (U.S. dollars) in damage.

Here, we discuss the meteorological history of Ida and highlight some of the records that Ida set. Historical landfall records from 1851 to present are taken from the National Hurricane Center/Atlantic Oceanographic and Meteorological Laboratory archive (http://www.aoml.noaa.gov/hrd/hurdat/All_U.S._Hurricanes.html). Ida's observed values are taken from the Atlantic hurricane database (HURDAT2; Landsea and Franklin 2013) that is based on Beven et al. (2022).

Ida developed from a high-amplitude easterly wave, becoming a tropical depression at 1200 UTC on 26 August in the west-central Caribbean and intensifying into a tropical storm by 1800 UTC. Over the following 24 hours, Ida rapidly intensified from 35 kt (18 m s^{-1}) to 70 kt (36 m s^{-1}), while tracking northwestward in a light shear and warm water environment in the western Caribbean. Ida made two landfalls in Cuba as a Category 1 hurricane on 27 August, the first on the Isle of Youth and the second on Pinar Del Rio. Disruption of Ida's circulation due to land interaction and dry air entrainment temporarily arrested Ida from strengthening, and it remained a Category 1 hurricane through 28 August.

As Ida continued northwest, vertical wind shear relaxed as the hurricane tracked over a warm eddy in the east-central Gulf of Mexico, causing rapid intensification. Between 1200 UTC on 28 August and 1200 UTC on 29 August, Ida's maximum sustained winds increased by 60 kt (31 m s^{-1}), from 70 kt (36 m s^{-1}) to 130 kt (67 m s^{-1}). This 60-kt intensification in 24 hours slightly exceeded Hurricane Laura (2020)'s rate of 55 kt (28 m s^{-1}) in 24 hours in the Gulf of Mexico. Laura also made landfall over Louisiana as a 130 kt (67 m s^{-1}) hurricane in late August. During this same time period, Ida's minimum central pressure fell 57 hPa (from 986 hPa to 929 hPa). At the peak of its intensification, Ida's pressure per aircraft reconnaissance fell by ~11 hPa in one hour between 1000 UTC and 1100 UTC on 29 August. Ida maintained a 130-kt intensity until initial landfall near Port Fourchon, Louisiana at ~1655 UTC on 29 August (Fig. SB4.1).

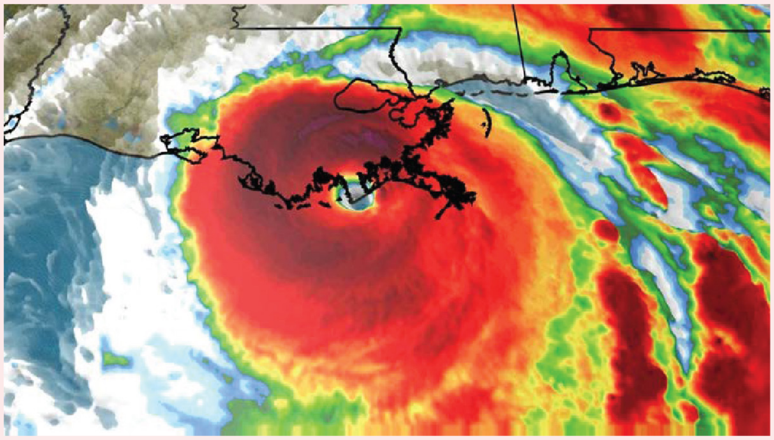

Fig. SB4.1. Infrared satellite image of Hurricane Ida at the time of its landfall at ~1655 UTC on 29 Aug 2021. Image courtesy of NOAA.

Following landfall, Ida only slowly weakened. Ida maintained Category 3+ hurricane intensity for at least five hours and Category 1+ hurricane intensity for at least 11 hours following initial landfall. This is likely due to a combination of factors, including a slow forward motion that kept part of Ida's circulation over water for most of 29 August and elevated soil moisture due to heavy antecedent rainfall over southern Louisiana. The system weakened to a tropical storm by mid-day on 30 August as it accelerated northeast over Mississippi, and it became a tropical depression on 31 August.

Ida was officially declared post-tropical while located over West Virginia on 1 September. However, as a post-tropical cyclone, Ida interacted with a frontal zone and produced copious rainfall (Fig. SB4.2), several violent tornadoes, and devastating flash flooding across the northern mid-Atlantic and southern New England. Flooding was particularly severe in and around the New York City metropolitan area, where widespread rainfall totals of 150–250 mm were recorded, including a 1-hour accumulation of 80 mm in New York's Central Park between ~0100 and 0200 UTC on 2 September. The estimated return period for 12-hour rainfall totals as observed from post-tropical Ida from the northern suburbs of Philadelphia northeast into coastal Connecticut is generally 100 to 200 years, with locally higher return periods. The final advisory on post-tropical Ida was issued on 2 September.

Hurricane Ida caused tremendous damage in southern Louisiana, with loss estimates in Louisiana of ~$55 billion (U.S. dollars), according to Beven et al. (2022). Flash flooding in the mid-Atlantic states was responsible for an additional ~$205 million in damage. Ida caused 55 direct and 32 indirect fatalities in the United States, and its precursor disturbance also caused significant flooding in Venezuela, which led to 20 fatalities. Storm surge exceeding three meters was reported to the east of where Ida made landfall. Ida's strong winds also led to extensive power outages, with over one million residents in Louisiana reported without electricity at one point.

Ida's 130 kt (67 m s^{-1}) intensity at landfall ties the Last Island Hurricane (1856) and Hurricane Laura (2020) for the strongest maximum sustained winds for a Louisiana landfalling hurricane on record. These sustained winds also equaled the fifth strongest on record for the continental United States. Ida's landfall pressure of 931 hPa was the second lowest for a Louisiana hurricane on record, trailing only Katrina (920 hPa), which struck on the same date 16 years prior to Ida. Laura and Ida are also the first two 130+ kt hurricanes on record to make landfall in the continental United States in consecutive years. The continental United States has now experienced three 130+ kt hurricane landfalls in the past four years: Michael (2018), Laura (2020), and Ida (2021). This equals the three 130+ kt hurricane landfalls recorded in the previous 82 years, 1936–2017: Camille (1969), Andrew (1992), and Charley (2004).

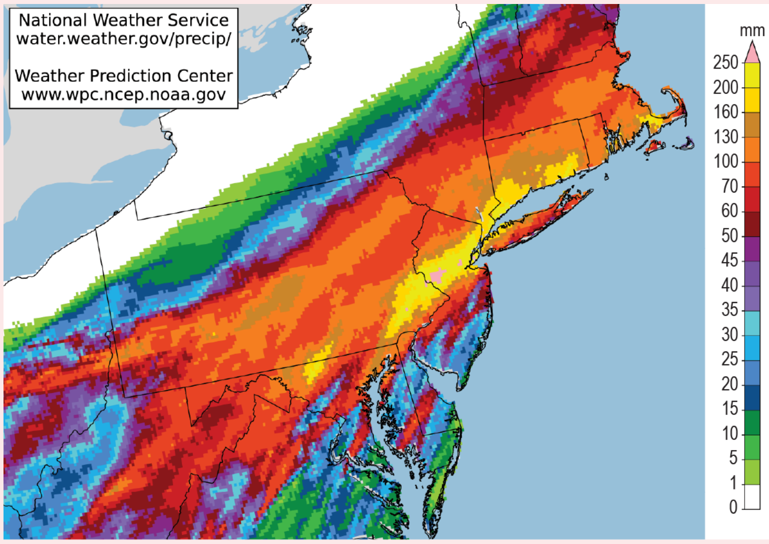

Fig. SB4.2. 48-h radar-estimated rainfall (mm) across the mid-Atlantic states and southern New England ending at 1200 UTC on 2 Sept 2021. Image courtesy of Gregory Carbin, NOAA/Weather Prediction Center.

References

Aiyyer, A., and J. Molinari, 2008: MJO and tropical cyclogenesis in the Gulf of Mexico and eastern Pacific: Case study and idealized numerical modeling. *J. Atmos. Sci.*, **65**, 2691–2704, https://doi.org/10.1175/2007JAS2348.1.

Aon, 2021a: Global Catastrophe Recap, August 2021, 19 pp, http://thoughtleadership.aon.com/Documents/20210009_analytics-if-august-global-recap.pdf.

——, 2021b: Global Catastrophe Recap, September 2021, 22 pp, http://thoughtleadership.aon.com/Documents/20210012-analytics-if-september-global-recap.pdf.

——, 2022: Global Catastrophe Recap, December 2021, 23 pp, https://www.aon.com/reinsurance/getmedia/e5d555d8-ade5-4fc4-b4b2-24ddad4bfb3d/20220124-analytics-if-december-global-recap.pdf.aspx.

Balaguru, K., P. Chang, R. Saravanan, L. R. Leung, Z. Xu, M. Li, and J. S. Hsieh, 2012: Ocean barrier layers' effect on tropical cyclone intensification. *Proc. Natl. Acad. Sci. USA*, **109**, 142343–142347, https://doi.org/10.1073/pnas.1201364109.

Banzon, V. F., and R. W. Reynolds, 2013: Use of WindSat to extend a microwave-based daily optimum interpolation sea surface temperature time series. *J. Climate*, **26**, 2557–2562, https://doi.org/10.1175/JCLI-D-12-00628.1.

Baxter, S., S. Weaver, J. Gottschalck, and Y. Xue, 2014: Pentad evolution of wintertime impacts of the Madden–Julian oscillation over the contiguous United States. *J. Climate*, **27**, 7356–7367, https://doi.org/10.1175/JCLI-D-14-00105.1.

Behringer, D. W., 2007: The Global Ocean Data Assimilation System (GODAS) at NCEP. *11th Symp. on Integrated Observing and Assimilation Systems for Atmosphere, Oceans, and Land Surface*, San Antonio, TX, Amer. Meteor. Soc., 3.3, http://ams.confex.com/ams/87ANNUAL/techprogram/paper_119541.htm.

——, M. Ji, and A. Leetmaa, 1998: An improved coupled model for ENSO prediction and implications for ocean initialization. Part I: The ocean data assimilation system. *Mon. Wea. Rev.*, **126**, 1013–1021, https://doi.org/10.1175/1520-0493(1998)126<1013:AICMFE>2.0.CO;2.

Bell, G. D., and M. Chelliah, 2006: Leading tropical modes associated with interannual and multi-decadal fluctuations in North Atlantic hurricane activity. *J. Climate*, **19**, 590–612, https://doi.org/10.1175/JCLI3659.1.

——, and Coauthors, 2000: The 1999 North Atlantic Hurricane season [in "Climate Assessment for 1999"]. *Bull. Amer. Meteor. Soc.*, **81** (6), S19–S22, https://doi.org/10.1175/1520-0477(2000)81[s1:CAF]2.0.CO;2.

——, E. S. Blake, C. W. Landsea, C. Wang, J. Schemm, T. Kimberlain, R. J. Pasch, and S. B. Goldenberg, 2017: Atlantic basin [in "State of the Climate in 2016"]. *Bull. Amer. Meteor. Soc.*, **98** (8), S108–S112, https://doi.org/10.1175/2017BAMSStateoftheClimate.1.

——, ——, ——, S. B. Goldenberg, and R. J. Pasch, 2018: Atlantic basin [in "State of the Climate in 2017"]. *Bull. Amer. Meteor. Soc.*, **99** (8), S114–S118, https://doi.org/10.1175/2018BAMSStateoftheClimate.1.

——, ——, ——, H. Wang, S. B. Goldenberg, and R. J. Pasch 2019: Atlantic basin [in "State of the Climate in 2018"]. *Bull. Amer. Meteor. Soc.*, **100** (9), S113–S119, https://doi.org/10.1175/2019BAMSStateoftheClimate.1.

——, E. S. Blake, C. W. Landsea, M. Rosencrans, H. Wang, S. B. Goldenberg, and R. J. Pasch, 2020: Atlantic basin [in "State of the Climate in 2019"]. *Bull. Amer. Meteor. Soc.*, **101** (7), S204–S212, https://doi.org/10.1175/BAMS-D-20-0077.1.

Berg, R., 2022: Hurricane Rick (EP172021). National Hurricane Center Tropical Cyclone Rep., 21 pp., https://www.nhc.noaa.gov/data/tcr/EP172021_Rick.pdf.

Beven, J., A. Hagen, and R. Berg, 2022: Hurricane Ida (AL092021). National Hurricane Center Tropical Cyclone Rep., 163 pp., https://www.nhc.noaa.gov/data/tcr/AL092021_Ida.pdf.

Camargo, S. J., and A. H. Sobel, 2005: Western North Pacific tropical cyclone intensity and ENSO. *J. Climate*, **18**, 2996–3006, https://doi.org/10.1175/JCLI3457.1.

——, A. W. Robertson, S. J. Gaffney, P. Smyth, and M. Ghil, 2007a: Cluster analysis of typhoon tracks: Part II: Large-scale circulation and ENSO. *J. Climate*, **20**, 3654–3676, https://doi.org/10.1175/JCLI4203.1.

——, K. A. Emanuel, and A. H. Sobel, 2007b: Use of a genesis potential index to diagnose ENSO effects on tropical cyclone genesis. *J. Climate*, **20**, 4819–4834, https://doi.org/10.1175/JCLI4282.1.

——, M. C. Wheeler, and A. H. Sobel, 2009: Diagnosis of the MJO modulation of tropical cyclogenesis using an empirical index. *J. Atmos. Sci.*, **66**, 3061–3074, https://doi.org/10.1175/2009JAS3101.1.

Cangialosi, J. P., 2021a: Hurricane Felicia (EP062021). National Hurricane Center Tropical Cyclone Rep., 15 pp., https://www.nhc.noaa.gov/data/tcr/EP062021_Felicia.pdf.

——, 2021b: Hurricane Pamela (EP162021). National Hurricane Center Tropical Cyclone Rep., 17 pp., https://www.nhc.noaa.gov/data/tcr/EP162021_Pamela.pdf.

Cassou, C., 2008: Intraseasonal interaction between the Madden–Julian Oscillation and the North Atlantic Oscillation. *Nature*, **455**, 523–527, https://doi.org/10.1038/nature07286.

Chia, H. H., and C. F. Ropelewski, 2002: The interannual variability in the genesis location of tropical cyclones in the northwest Pacific. *J. Climate*, **15**, 2934–2944, https://doi.org/10.1175/1520-0442(2002)015<2934:TIVITG>2.0.CO;2.

Chen, L., and J.-J. Luo, 2021: Indian Ocean dipole [in "State of the Climate in 2020"]. *Bull. Amer. Meteor. Soc.*, **103** (8), S21–S25, https://doi.org/10.1175/BAMS-D-21-00090.1.

Dare, R. A., and J. L. McBride, 2011: Sea surface temperature response to tropical cyclones. *Mon. Wea. Rev.*, **139**, 3798–3808, https://doi.org/10.1175/MWR-D-10-05019.1.

Diamond, H. J., and J. A. Renwick, 2015: The climatological relationship between tropical cyclones in the southwest Pacific and the Madden–Julian Oscillation. *Int. J. Climatol.*, **35**, 676–686, https://doi.org/10.1002/joc.4012.

——, and C. J. Schreck III , Eds., 2019: The tropics [in "State of the Climate in 2018"]. *Bull. Amer. Meteor. Soc.*, **100** (9), S101–S140, https://doi.org/10.1175/2019BAMSStateoftheClimate.1.

——, and ——, Eds, 2020: The tropics [in "State of the Climate in 2019"]. *Bull. Amer. Meteor. Soc.*, **100** (8), S185–S238, https://doi.org/10.1175/BAMS-D-20-0077.1.

——, and ——, Eds., 2021: The tropics [in "State of the Climate in 2020"]. *Bull. Amer. Meteor. Soc.*, **102** (8), S199–S262, https://doi.org/10.1175/BAMS-D-21-0080.1.

——, A. M. Lorrey, K. R. Knapp, and D. H. Levinson, 2012: Development of an enhanced tropical cyclone tracks database for the southwest Pacific from 1840 to 2011. *Int. J. Climatol.*, **32**, 2240–2250, https://doi.org/10.1002/joc.2412.

Ding, Q., E. J. Steig, D. S. Battisti, and J. M. Wallace, 2012: Influence of the tropics on the southern annular mode. *J. Climate*, **25**, 6330–6348, https://doi.org/10.1175/JCLI-D-11-00523.1.

Domingues, R., and Coauthors, 2015: Upper ocean response to Hurricane Gonzalo (2014): Salinity effects revealed by targeted and sustained underwater glider observations. *Geophys. Res. Lett.*, **42**, 7131–7138, https://doi.org/10.1002/2015GL065378.

Dube, S. K., D. Rao, P. C. Sinha, T. S. Murty, and N. Bahuluyan, 1997: Storm surge in the Bay of Bengal and Arabian Sea: The problem and its prediction. *Mausam*, **48**, 283–304, https://doi.org/10.54302/mausam.v48i2.4012.

Ebita, A., and Coauthors, 2011: The Japanese 55-year Reanalysis "JRA-55": An interim report. *SOLA*, **7**, 149–152, https://doi.org/10.2151/sola.2011-038.

Emanuel, K. A., 1988: The maximum intensity of hurricanes. *J. Atmos. Sci.*, **45**, 1143–1155, https://doi.org/10.1175/1520-0469(1988)045<1143:TMIOH>2.0.CO;2.

——, and D. S. Nolan, 2004: Tropical cyclone activity and the global climate system. *26th Conf. on Hurricanes and Tropical Meteorology*, Miami, FL, Amer. Meteor. Soc., 10A.2, https://ams.confex.com/ams/26HURR/techprogram/paper_75463.htm.

Enfield, D. B., and A. M. Mestas-Nuñez, 1999: Multiscale variabilities in global sea surface temperatures and their relationships with tropospheric climate patterns. *J. Climate*, **12**, 2719–2733, https://doi.org/10.1175/1520-0442(1999)012<2719:MVIGSS>2.0.CO;2.

Feng, M., M. J. McPhaden, S. Xie, and J. Hafner, 2013: La Niña forces unprecedented Leeuwin Current warming in 2011. *Sci. Rep.*, **3**, 1277. https://doi.org/10.1038/srep01277.

Frank, W. M., and P. E. Roundy, 2006: The role of tropical waves in tropical cyclogenesis. *Mon. Wea. Rev*., **134**, 2397–2417, https://doi.org/10.1175/MWR3204.1.

Gill, A. E., 1980: Some simple solutions for heat-induced tropical circulation. *Quart. J. Roy. Meteor. Soc*., **106**, 447–462, https://doi.org/10.1002/qj.49710644905.

Goldenberg, S. B., and L. J. Shapiro, 1996: Physical mechanisms for the association of El Niño and West African rainfall with Atlantic major hurricane activity. *J. Climate*, **9**, 1169–1187, https://doi.org/10.1175/1520-0442(1996)009<1169:PMFTAO>2.0.CO;2.

——, C. W. Landsea, A. M. Mestas-Nuñez, and W. M. Gray, 2001: The recent increase in Atlantic hurricane activity: Causes and implications. *Science*, **293**, 474–479, https://doi.org/10.1126/science.1060040.

Goni, G. J., and Coauthors, 2009: Applications of satellite-derived ocean measurements to tropical cyclone intensity forecasting. *Oceanography*, **22**, 190–197, https://doi.org/10.5670/oceanog.2009.78.

——, and Coauthors, 2017: Autonomous and Lagrangian ocean observations for Atlantic tropical cyclone studies and forecasts. *Oceanography*, **30**, 92–103, https://doi.org/10.5670/oceanog.2017.227.

Gray, W. M., 1990: Strong association between West African rainfall and U.S. landfall of intense hurricanes. *Science*, **249**, 1251–1256, https://doi.org/10.1126/science.249.4974.1251.

Guo, Y., X. Jiang, and D. E. Waliser, 2014: Modulation of the convectively coupled Kelvin waves over South America and the tropical Atlantic Ocean in association with the Madden–Julian Oscillation. *J. Atmos. Sci.*, **71**, 1371–1388, https://doi.org/10.1175/JAS-D-13-0215.1.

Hastenrath, S., 1990: Decadal-scale changes of the circulation in the tropical Atlantic sector associated with Sahel drought. *Int. J. Climatol.*, **10**, 459–472, https://doi.org/10.1002/joc.3370100504.

Hendon, H., C. Zhang, and J. Glick, 1999: Interannual variation of the Madden–Julian oscillation during austral summer. *J. Climate*, **12**, 2538–2550, https://doi.org/10.1175/1520-0442(1999)012<2538:IVOTMJ>2.0.CO;2.

Hersbach, H., and Coauthors, 2020: The ERA5 global reanalysis. *Quart. J. Roy. Meteor. Soc.*, **146**, 1999–2049, https://doi.org/10.1002/qj.3803.

Hong, C.-C., T. Li, and J.-J. Luo, 2008: Asymmetry of the Indian Ocean Dipole. Part II: Model diagnosis. *J. Climate*, **21**, 4849–4858.

Huang, B., and Coauthors, 2017: Extended Reconstructed Sea Surface Temperature, version 5 (ERSSTv5): Upgrades, validations, and intercomparisons. *J. Climate*, **30**, 8179–8205, https://doi.org/10.1175/JCLI-D-16-0836.1.

Huang, B., C. Liu, V. Banzon, E. Freeman, G. Graham, B. Hankins, T. Smith, and H.-M. Zhang, 2020: Improvements of the Daily Optimum Interpolation Sea Surface Temperature (DOISST) version 2.1. *J. Climate*, **34**, 2923–2939, https://doi.org/10.1175/JCLI-D-20-0166.1.

Huffman, G. J., R. F. Adler, D. T. Bolvin, and G. Gu, 2009: Improving the global precipitation record: GPCP version 2.1. *Geophys. Res. Lett.*, **36**, L17808, https://doi.org/10.1029/2009GL040000.

IMD, 2021: Extremely Severe Cyclonic Storm TAUKTAE over the Arabian Sea (14th–19th May, 2021): A report. India Meteorological Department, 64 pp., https://rsmcnewdelhi.imd.gov.in/uploads/report/26/26_e0cc1a_Preliminary%20Report%20on%20ESCS%20TAUKTAE-19july.pdf.

Kalnay, E., and Coauthors, 1996: The NCEP/NCAR 40-Year Reanalysis Project. *Bull. Amer. Meteor. Soc.*, **77**, 437–471, https://doi.org/10.1175/1520-0477(1996)077<0437:TNYRP>2.0.CO;2.

Kayano, M., and V. Kousky, 1999: Intraseasonal (30–60 day) variability in the global tropics: Principal modes and their evolution. *Tellus*, **51**, 373–386, https://doi.org/10.3402/tellusa.v51i3.13459.

Kiladis, G. N., and K. M. Weickmann, 1992: Circulation anomalies associated with tropical convection during northern winter. *Mon. Wea. Rev.*, **120**, 1900–1923, https://doi.org/10.1175/1520-0493(1992)120<1900:CAAWTC>2.0.CO;2.

——, K. H. Straub, and P. T. Haertel, 2005: Zonal and vertical structure of the Madden–Julian oscillation. *J. Atmos. Sci.*, **62**, 2790–2809, https://doi.org/10.1175/JAS3520.1.

——, M. C. Wheeler, P. T. Haertel, K. H. Straub, and P. E. Roundy, 2009: Convectively coupled equatorial waves. *Rev. Geophys.*, **47**, RG2003, https://doi.org/10.1029/2008RG000266.

Klotzbach, P. J., K. M. Wood, C. J. Schreck III, S. G. Bowen, C. M. Patricola, and M. M. Bell, 2022: Trends in global tropical cyclone activity: 1990–2021. *Geophys. Res. Lett.*, **49**, e2021GL095774, https://doi.org/10.1029/2021GL095774.

Knaff, J. A., C. R. Sampson, and K. D. Musgrave, 2018: An operational rapid intensification prediction aid for the western North Pacific. *Wea. Forecasting*, **33**, 799–811, https://doi.org/10.1175/WAF-D-18-0012.1.

Knapp, K. R., M. C. Kruk, D. H. Levinson, H. J. Diamond, and C. J. Neumann, 2010: The International Best Track Archive for Climate Stewardship (IBTrACS): Unifying tropical cyclone data. *Bull. Amer. Meteor. Soc.*, **91**, 363–376, https://doi.org/10.1175/2009BAMS2755.1.

——, J. A. Knaff, C. R. Sampson, G. M. Riggio, and A. D. Schnapp, 2013: A pressure-based analysis of the historical western North Pacific tropical cyclone intensity record. *Mon. Wea. Rev.*, **141**, 2611–2631, https://doi.org/10.1175/MWR-D-12-00323.1.

Knutson, T. R., and K. M. Weickmann, 1987: 30–60 day atmospheric oscillations: Composite life cycles of convection and circulation anomalies. *Mon. Wea. Rev.*, **115**, 1407–1436, https://doi.org/10.1175/1520-0493(1987)115<1407:DAOCLC>2.0.CO;2.

Kousky, V. E., and M. T. Kayano, 1994: Principal modes of outgoing longwave radiation and 250-mb circulation for the South American sector. *J. Climate*, **7**, 1131–1143, https://doi.org/10.1175/1520-0442(1994)007<1131:PMOOLR>2.0.CO;2.

Krishnamurti, T. N., and D. Subrahmanyam, 1982: The 30–50 day mode at 850 mb during MONEX. *J. Atmos. Sci.*, **39**, 2088–2095, https://doi.org/10.1175/1520-0469(1982)039<2088:TDMAMD>2.0.CO;2.

Landsea, C. W., and J. L. Franklin, 2013: Atlantic hurricane database uncertainty and presentation of a new database format. *Mon. Wea. Rev.*, **141**, 3576–3592, https://doi.org/10.1175/MWR-D-12-00254.1.

——, W. M. Gray, P. W. Mielke, and K. J. Berry, 1992: Long-term variations of western Sahelian monsoon rainfall and intense U.S. landfalling hurricanes. *J. Climate*, **5**, 1528–1534, https://doi.org/10.1175/1520-0442(1992)005<1528:LTVOWS>2.0.CO;2.

——, G. D. Bell, W. M. Gray, and S. B. Goldenberg, 1998: The extremely active 1995 Atlantic hurricane season: Environmental conditions and verification of seasonal forecasts. *Mon. Wea. Rev.*, **126**, 1174–1193, https://doi.org/10.1175/1520-0493(1998)126<1174:TEAAHS>2.0.CO;2.

——, G. A. Vecchi, L. Bengtsson, and T. R. Knutson, 2010: Impact of duration thresholds on Atlantic tropical cyclone counts. *J. Climate*, **23**, 2508–2519, https://doi.org/10.1175/2009JCLI3034.1.

Latto, A., 2021: Hurricane Enrique (EP052021). National Hurricane Center Tropical Cyclone Rep., 20 pp., https://www.nhc.noaa.gov/data/tcr/EP052021_Enrique.pdf.

——, 2022: Hurricane Olaf (EP152021). National Hurricane Center Tropical Cyclone Rep., 21 pp., https://www.nhc.noaa.gov/data/tcr/EP152021_Olaf.pdf.

Lau, W. K.-M., and D. E. Waliser, 2012: *Intraseasonal Variability in the Atmosphere-Ocean Climate System*. Springer, 642 pp.

Leipper, D. F., and D. Volgenau, 1972: Hurricane heat potential of the Gulf of Mexico. *J. Phys. Oceanogr.*, **2**, 218–224, https://doi.org/10.1175/1520-0485(1972)002<0218:HHPOTG>2.0.CO;2.

Liebmann, B., and C. A. Smith, 1996: Description of a complete (interpolated) outgoing longwave radiation dataset. *Bull. Amer. Meteor. Soc.*, **77**, 1275–1277, https://doi.org/10.1175/1520-0477-77.6.1274.

Lin, I. I., and Coauthors, 2013: An ocean coupling potential intensity index for tropical cyclones. *Geophys. Res. Lett.*, **40**, 1878–1882, https://doi.org/10.1002/grl.50091.

Lin, H., G. Brunet, and J. Derome, 2009: An observed connection between the North Atlantic oscillation and the Madden–Julian oscillation. *J. Climate*, **22**, 364–380, https://doi.org/10.1175/2008JCLI2515.1.

——, I.-F. Pun, and C.-C. Lien, 2014: "Category-6" Supertyphoon Haiyan in global warming hiatus: Contribution from subsurface ocean warming. *Geophys. Res. Lett.*, **41**, 8547–8553, https://doi.org/10.1002/2014GL061281.

——, and Coauthors, 2020: ENSO and tropical cyclones. *El Niño Southern Oscillation in a Changing Climate, Geophys. Monogr.*, Vol. 253, Amer. Geophys. Union, 377–408, https://doi.org/10.1002/9781119548164.ch17.

Liu, T., J. Li, C. Sun, T. Lian, and Y. Zhang, 2021: Impact of the April–May SAM on central Pacific Ocean sea temperature over the following three seasons. *Climate Dyn.*, **57**, 775–786, https://doi.org/10.1007/s00382-021-05738-4.

Luo, J.-J., 2017: Indian Ocean dipole [in "State of the Climate in 2016"]. *Bull. Amer. Meteor. Soc.*, **98** (8), S126–S128, https://doi.org/10.1175/2017BAMSStateoftheClimate.1.

——, S. Masson, S. Behera, and T. Yamagata, 2007: Experimental forecasts of the Indian Ocean Dipole using a coupled OAGCM. *J. Climate*, **20**, 2178–2190, https://doi.org/10.1175/JCLI4132.1.

——, R. Zhang, S. K. Behera, Y. Masumoto, F.-F. Jin, R. Lukas, and T. Yamagata, 2010: Interaction between El Niño and extreme Indian Ocean dipole. *J. Climate*, **23**, 726–742, https://doi.org/10.1175/2009JCLI3104.1.

——, W. Sasaki, and Y. Masumoto, 2012: Indian Ocean warming modulates Pacific climate change. *Proc. Natl. Acad. Sci. USA*, **109**, 18 701–18 706, https://doi.org/10.1073/pnas.1210239109.

Madden, R., and P. Julian, 1971: Detection of a 40–50 day oscillation in the zonal wind in the tropical Pacific. *J. Atmos. Sci.*, **28**, 702–708, https://doi.org/10.1175/1520-0469(1971)028<0702:DOADOI>2.0.CO;2.

——, and ——, 1972: Description of global-scale circulation cells in the tropics with a 40–50 day period. *J. Atmos. Sci.*, **29**, 1109–1123, https://doi.org/10.1175/1520-0469(1972)029<1109:DOGSCC>2.0.CO;2.

——, and ——, 1994: Observations of the 40–50-day tropical oscillation: A review. *Mon. Wea. Rev.*, **122**, 814–837, https://doi.org/10.1175/1520-0493(1994)122<0814:OOTDTO>2.0.CO;2.

Magee, A. D., A. S. Kiem, and A. M. Lorrey, 2022: Insights into the usefulness of a new extreme weather guidance tool: The Long-Range Tropical Cyclone Outlook for the Southwest Pacific (TCO-SP). *Bull. Amer. Meteor. Soc.*, **103**, E1220–E1233, https://doi.org/10.1175/BAMS-D-21-0108.1.

Mainelli, M., M. DeMaria, L. Shay, and G. Goni, 2008: Application of oceanic heat content estimation to operational forecasting of recent Atlantic category 5 hurricanes. *Wea. Forecasting*, **23**, 3–16, https://doi.org/10.1175/2007WAF2006111.1.

Maloney, E. D., and D. L. Hartmann, 2001: The Madden–Julian Oscillation, barotropic dynamics, and North Pacific tropical cyclone formation. Part I: Observations. *J. Atmos. Sci.*, **58**, 2545–2558, https://doi.org/10.1175/1520-0469(2001)058<2545:TMJOBD>2.0.CO;2.

Matsuno, T., 1966: Quasi-geostrophic motions in the equatorial area. *J. Meteor. Soc. Japan*, **44**, 25–43, https://doi.org/10.2151/jmsj1965.44.1_25.

Matthews, A. J., 2008: Primary and successive events in the Madden–Julian Oscillation. *Quart. J. Roy. Meteor. Soc.*, **134**, 439–453, https://doi.org/10.1002/qj.224.

Mo, K. C., 2000: The association between intraseasonal oscillations and tropical storms in the Atlantic Basin. *Mon. Wea. Rev.*, **128**, 4097–4107, https://doi.org/10.1175/1520-0493(2000)129<4097:TABIOA>2.0.CO;2.

——, and V. E. Kousky, 1993: Further analysis of the relationship between circulation anomaly patterns and tropical convection. *J. Geophys. Res.*, **98**, 5103–5113, https://doi.org/10.1029/92JD02952.

Moreno, P. I., and Coauthors, 2018: Onset and evolution of southern annular mode-like changes at centennial timescale. *Sci. Rep.*, **8**, 3458, https://doi.org/10.1038/s41598-018-21836-6.

Münnich, M., and J. D. Neelin, 2005: Seasonal influence of ENSO on the Atlantic ITCZ and equatorial South America. *Geophys. Res. Lett.*, **32**, L21709, https://doi.org/10.1029/2005GL023900.

NOAA, 2020: El Niño/Southern Oscillation (ENSO) diagnostic discussion. NOAA/NWS, 10 September, https://www.cpc.ncep.noaa.gov/products/analysis_monitoring/enso_disc_sep2020/ensodisc.shtml.

——, 2021: El Niño/Southern Oscillation (ENSO) diagnostic discussion. NOAA/NWS, 12 August, https://www.cpc.ncep.noaa.gov/products/analysis_monitoring/enso_disc_aug2021/ensodisc.shtml.

Nobre, P., and J. Shukla, 1996: Variations of sea surface temperature, wind stress and rainfall over the tropical Atlantic and South America. *J. Climate*, **9**, 2464–2479, https://doi.org/10.1175/1520-0442(1996)009<2464:VOSSTW>2.0.CO;2.

Papin, P. P., 2022: Tropical Storm Dolores (EP042021). National Hurricane Center Tropical Cyclone Rep., 20 pp., https://www.nhc.noaa.gov/data/tcr/EP042021_Dolores.pdf.

Pezza, A. B., and A. S. Coelho, 2021: Atlantic [in "State of the Climate in 2020"]. *Bull. Amer. Meteor. Soc.*, **102** (9), S215–S216, https://doi.org/10.1175/BAMS-D-21-0080.1.

Raga, G. B., B. Bracamontes-Ceballos, L. Farfán, and R. Romero-Centeno, 2013: Landfalling tropical cyclones on the Pacific coast of Mexico: 1850–2010. *Atmósfera*, **26**, 209–220, https://doi.org/10.1016/S0187-6236(13)71072-5.

Ramage, C. S., 1971: *Monsoon Meteorology*. Academic Press, 296 pp.

Reinhart, B. J., D. Wroe, and S. Houston, 2021: Hurricane Linda (EP122021). National Hurricane Center Tropical Cyclone Rep.,19 pp., https://www.nhc.noaa.gov/data/tcr/EP122021_Linda.pdf.

Reynolds, R. W., N. A. Rayner, T. M. Smith, D. C. Stokes, and W. Wang, 2002: An improved in situ and satellite SST analysis for climate. *J. Climate*, **15**, 1609–1625, https://doi.org/10.1175/1520-0442(2002)015<1609:AIISAS>2.0.CO;2.

Riddle, E., M. Stoner, N. Johnson, M. L'Heureux, D. Collins, and S. Feldstein, 2013: The impact of the MJO on clusters of wintertime circulation anomalies over the North American region. *Climate Dyn.*, 40, 1749–1766, https://doi.org/10.1007/s00382-012-1493-y.

Ropelewski, C. F., and M. S. Halpert, 1987: Global and regional scale precipitation patterns associated with the El Niño–Southern Oscillation. *Mon. Wea. Rev.*, **115**, 1606–1626, https://doi.org/10.1175/1520-0493(1987)115<1606:GARSPP>2.0.CO;2.

——, and ——, 1989: Precipitation patterns associated with the high index phase of the Southern Oscillation. *J. Climate*, **2**, 268–284, https://doi.org/10.1175/1520-0442(1989)002<0268:PPAWTH>2.0.CO;2.

Saha, S., and Coauthors, 2014: The NCEP Climate Forecast System version 2. *J. Climate*, **27**, 2185–2208, https://doi.org/10.1175/JCLI-D-12-00823.1.

Saji, N. H., B. N. Goswami, P. N. Vinayachandran, and T. Yamagata, 1999: A dipole mode in the tropical Indian ocean. *Nature*, **401**, 360–363, https://doi.org/10.1038/43854.

Schneider, T., T. Bischoff, and G. H. Haug, 2014: Migrations and dynamics of the intertropical convergence zone. *Nature*, **513**, 45–53, https://doi.org/10.1038/nature13636.

Schreck, C. J., 2015: Kelvin waves and tropical cyclogenesis: A global survey. *Mon. Wea. Rev.*, **143**, 3996–4011, https://doi.org/10.1175/MWR-D-15-0111.1.

——, 2016: Convectively coupled Kelvin waves and tropical cyclogenesis in a semi-Lagrangian framework. *Mon. Wea. Rev.*, **144**, 4131–4139, https://doi.org/10.1175/MWR-D-16-0237.1.

——, and J. Molinari, 2011: Tropical cyclogenesis associated with Kelvin waves and the Madden–Julian oscillation. *Mon. Wea. Rev.*, **139**, 2723–2734, https://doi.org/10.1175/MWR-D-10-05060.1.

——, ——, and A. Aiyyer, 2012: A global view of equatorial waves and tropical cyclogenesis. *Mon. Wea. Rev.*, **140**, 774–788, https://doi.org/10.1175/MWR-D-11-00110.1.

——, J. M. Cordeira, and D. Margolin, 2013: Which MJO events affect North American temperatures? *Mon. Wea. Rev.*, **141**, 3840–3850, https://doi.org/10.1175/MWR-D-13-00118.1.

——, K. R. Knapp, and J. P. Kossin, 2014: The impact of best track discrepancies on global tropical cyclone climatologies using IBTrACS. *Mon. Wea. Rev.*, **142**, 3881–3899, https://doi.org/10.1175/MWR-D-14-00021.1.

——, H.-T. Lee, and K. R. Knapp, 2018: HIRS outgoing longwave radiation—Daily climate data record: Application toward identifying tropical subseasonal variability. *Remote Sens.*, **10**, 1325, https://doi.org/10.3390/rs10091325.

Shay, L. K., G. J. Goni, and P. G. Black, 2000: Effects of a warm oceanic feature on Hurricane Opal. *Mon. Wea. Rev.*, **128**, 1366–1383, https://doi.org/10.1175/1520-0493(2000)128<1366:EOAWOF>2.0.CO;2.

Smith, T. M., R. W. Reynolds, T. C. Peterson, and J. Lawrimore, 2008: Improvements to NOAA's historical merged land–ocean surface temperature analysis (1880–2006). *J. Climate*, **21**, 2283–2296, https://doi.org/10.1175/2007JCLI2100.1.

Vecchi, G. A., and B. J. Soden, 2007: Effect of remote sea surface temperature change on tropical cyclone potential intensity. *Nature*, **450**, 1066–1071, https://doi.org/10.1038/nature06423.

Ventrice, M. J., C. D. Thorncroft, and M. A. Janiga, 2012a: Atlantic tropical cyclogenesis: A three-way interaction between an African easterly wave, diurnally varying convection, and a convectively coupled atmospheric Kelvin wave. *Mon. Wea. Rev.*, **140**, 1108–1124, https://doi.org/10.1175/MWR-D-11-00122.1.

Ventrice, M. J., C. D. Thorncroft, and C. J. Schreck, 2012b: Impacts of convectively coupled Kelvin waves on environmental conditions for Atlantic tropical cyclogenesis. *Mon. Wea. Rev.*, **140**, 2198–2214, https://doi.org/10.1175/MWR-D-11-00305.1.

Villarini, G., G. A. Vecchi, T. R. Knutson, and J. A. Smith, 2011: Is the recorded increase in short duration North Atlantic tropical storms spurious? *J. Geophys. Res.*, **116**, D10114, https://doi.org/10.1029/2010JD015493.

Vincent, D. G., 1994: The South Pacific Convergence Zone (SPCZ): A review. *Mon. Wea. Rev.*, **122**, 1949–1970, https://doi.org/10.1175/1520-0493(1994)122<1949:TSPCZA>2.0.CO;2.

Waliser, D. E., and C. Gautier, 1993: A satellite-derived climatology of the ITCZ. *J. Climate*, **6**, 2162–2174, https://doi.org/10.1175/1520-0442(1993)006<2162:ASDCOT>2.0.CO;2.

Wang, B., 1994: Climatic regimes of tropical convection and rainfall. *J. Climate*, **7**, 1109–1118, https://doi.org/10.1175/1520-0442(1994)007<1109:CROTCA>2.0.CO;2.

——, and Q. Ding, 2008: Global monsoon: Dominant mode of annual variation in the tropics. *Dyn. Atmos. Ocean*, **44**, 165–183, https://doi.org/10.1016/j.dynatmoce.2007.05.002.

——, J. Liu, H. J. Kim, P. J. Webster, and S. Y. Yim, 2012: Recent change of the global monsoon precipitation (1979–2008). *Climate Dyn.*, **39**, 1123–1135, https://doi.org/10.1007/s00382-011-1266-z.

Wheeler, M. C., and G. N. Kiladis, 1999: Convectively coupled equatorial waves: Analysis of clouds and temperature in the wavenumber-frequency domain. *J. Atmos. Sci.*, **56**, 374–399, https://doi.org/10.1175/1520-0469(1999)056<0374:CCEWAO>2.0.CO;2.

——, and H. H. Hendon, 2004: An all-season real-time multivariate MJO index: Development of an index for monitoring and prediction. *Mon. Wea. Rev.*, **132**, 1917–1932, https://doi.org/10.1175/1520-0493(2004)132<1917:AARMMI>2.0.CO;2.

Wood, K. M., and E. A. Ritchie, 2015: A definition for rapid weakening in the North Atlantic and eastern North Pacific. *Geophys. Res. Lett.*, **42**, 10 091–10 097, https://doi.org/10.1002/2015GL066697.

——, and C. J. Schreck, 2020: Eastern North Pacific and Central North Pacific basins [in "State of the Climate in 2019"]. *Bull. Amer. Meteor. Soc.*, **101** (8), S212–S214, https://doi.org/10.1175/BAMS-D-20-0077.1.

——, and ——, 2021: Eastern North Pacific and Central North Pacific basins [in "State of the Climate in 2020"]. *Bull. Amer. Meteor. Soc.*, **102** (8), S233–S236, https://doi.org/10.1175/BAMS-D-21-0080.1.

Xie, P., and P. A. Arkin, 1997: Global precipitation: A 17-year monthly analysis based on gauge observations, satellite estimates, and numerical model outputs. *Bull. Amer. Meteor. Soc.*, **78**, 2539–2558, https://doi.org/10.1175/1520-0477(1997)078<2539:GPAYMA>2.0.CO;2.

Yim, S. Y., B. Wang, J. Liu, and Z. W. Wu, 2014: A comparison of regional monsoon variability using monsoon indices. *Climate Dyn.*, **43**, 1423–1437, https://doi.org/10.1007/s00382-013-1956-9.

Zhang, C., 2005: Madden–Julian oscillation. *Rev. Geophys.*, **43**, RG2003, https://doi.org/10.1029/2004RG000158.

——, and J. Gottschalck, 2002: SST anomalies of ENSO and the Madden–Julian oscillation in the equatorial Pacific. *J. Climate*, **15**, 2429–2445, https://doi.org/10.1175/1520-0442(2002)015<2429:SAOEAT>2.0.CO;2.

Zhang, H.-M., and Coauthors, 2019: Updated temperature data give a sharper view of climate trends. *Eos*, **100**, https://doi.org/10.1029/2019EO128229.

Zheng, T., T. Feng, K. Xu, and X. Cheng, 2020: Precipitation and the associated moist static energy budget off Western Australia in conjunction with Ningaloo Niño. *Front. Earth Sci.*, **8**, https://doi.org/10.3389/feart.2020.597915

Zheng, Z.-W., I.-I. Lin, B. Wang, H.-C. Huang, and C.-H. Chen, 2015: A long neglected damper in the El Nino–typhoon relationship: A 'Gaia-like' process. *Sci. Rep.*, **5**, 11103, https://doi.org/10.1038/srep11103.